Since January 2020 Elsevier has created a COVID-19 resource centre with free information in English and Mandarin on the novel coronavirus COVID-19. The COVID-19 resource centre is hosted on Elsevier Connect, the company's public news and information website.

Elsevier hereby grants permission to make all its COVID-19-related research that is available on the COVID-19 resource centre - including this research content - immediately available in PubMed Central and other publicly funded repositories, such as the WHO COVID database with rights for unrestricted research re-use and analyses in any form or by any means with acknowledgement of the original source. These permissions are granted for free by Elsevier for as long as the COVID-19 resource centre remains active.

Building and Environment 232 (2023) 110066

Contents lists available at ScienceDirect

Building and Environment

journal homepage: www.elsevier.com/locate/buildenv

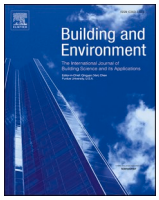

Transmission mitigation of COVID-19: Exhaled contaminants removal and energy saving in densely occupied space by impinging jet ventilation

Chao Qin [a], Shu-Zhen Zhang [b], Zheng-Tong Li [c], Chih-Yung Wen [c], Wei-Zhen Lu [a,*]

[a] Department of Architecture and Civil Engineering, City University of Hong Kong, Hong Kong Special Administrative Region
[b] Department of Building Environment and Energy Engineering, The Hong Kong Polytechnic University, Hong Kong Special Administrative Region
[c] Department of Aeronautical and Aviation Engineering, The Hong Kong Polytechnic University, Hong Kong Special Administrative Region

ARTICLE INFO

Keywords:
Densely occupied space
Impinging jet ventilation
Breathing air quality
Thermal comfort
Energy saving

ABSTRACT

The pandemic of COVID-19 and its transmission ability raise much attention to ventilation design as indoor-transmission outstrips outdoor-transmission. Impinging jet ventilation (IJV) systems might be promising to ventilate densely occupied large spaces due to their high jet momentum. However, their performances in densely occupied spaces have rarely been explored. This study proposes a modified IJV system and evaluates its performance numerically in a densely occupied classroom mockup. A new assessment formula is also proposed to evaluate the nonuniformity of target species CO_2. The infector is assumed as the manikin with the lowest tracer gas concentration in the head region. The main results include: a) Indoor air quality (IAQ) in the classroom is improved significantly compared with a mixing ventilation system, i.e., averaged CO_2 in the occupied zone (OZ) is reduced from 1287 ppm to 1078 ppm, the OZ-averaged mean age of air is reduced from 439 s to 177 s; b) The mean infection probability is reduced from 0.047% to 0.027% with an infector, and from 0.035% to 0.024% with another infector; c) Cooling coil load is reduced by around 21.0%; d) Overall evaluation indices meet the requirements for comfortable environments, i.e., the temperature difference between head and ankle is within 3 °C and the OZ-averaged predictive mean vote is in the range of −0.5 - 0.5; e) Thermal comfort level and uniformity are decreased, e.g., overcooling near diffuser at ankle level. Summarily, the target system effectively improves IAQ, reduces exhaled-contaminant concentration in head regions, and saves energy as well.

1. Introduction

The pandemic of COVID-19 raises concerns about indoor air quality (IAQ) more than ever because indoor transmission far outstrips outdoor transmission [1]. In a poorly ventilated restaurant, airborne transmission is claimed as the reason for the outbreak of COVID-19 between unrelated families because there is no close contact between these families, and the infection distribution matches the transportation of exhaled virus-laden contaminants [2]. At the same time, the basic reproduction number of the pandemic variant increases [3]. Therefore, it remains crucial to improve ventilation performance in the post-pandemic period or after the reopening of society [4,5]. Additionally, ventilation is vital to reduce the risk of various airborne transmission viruses, e.g., influenza virus, respiratory syncytial virus, and MERS-COV [6].

Densely occupied spaces (e.g., classrooms, restaurants, and cinemas) require great cooling demand and high contaminant removal efficiency due to their high intensity of heat load [7,8] and a high concentration of contaminants [9]. More importantly, they may cause cross-infection because of short social distance and a large number of susceptible people [10]. Many researchers tried to improve the ventilation performance for densely occupied spaces. Mikeska and Fan [7] proposed a porous ceiling as a diffuser to overcome the discomfort caused by high velocities when traditional diffusers were used in mixing ventilation (MV) systems. Wang et al. [11] and Yang et al. [12] studied performances of a displacement natural ventilation system resulting in improvements compared with traditional systems.

Personal ventilation systems and physical partitions are proposed as well. Fathollahzadeh et al. [13] and Shokrollahi et al. [14] applied underfloor air distribution (UFAD) systems to cool densely occupied spaces and mounted a diffuser for each occupant. Additionally, physical partitions are proposed during the COVID-19 pandemic. On the one hand, these partitions effectively reduce the risk of cross-infection in a classroom equipped with an MV system due to their obstructive effect on

* Corresponding author.
E-mail address: bcwzlu@cityu.edu.hk (W.-Z. Lu).

https://doi.org/10.1016/j.buildenv.2023.110066
Received 17 October 2022; Received in revised form 28 January 2023; Accepted 31 January 2023
Available online 3 February 2023
0360-1323/© 2023 Elsevier Ltd. All rights reserved.

airflows [15,16]. On the other hand, they may increase the exposure of latter diners in a densely occupied canteen for the same reason [17].

There are many drawbacks of previously proposed systems for daily densely occupied spaces (e.g., classrooms) in the reopened society when there is still a risk of infection. Firstly, personal ventilation systems might be limited because they are too expensive to be used in large numbers and can only ventilate a fixed small area while occupants may move around. Secondly, the supplied air might be hard to reach occupants at downstream rows when the supply momentum is low (e.g., displacement ventilation (DV), stratum ventilation (SV)). For instance, the horizontal supply jet for the SV system bends downwards [18], while the breathing zone for several rows of occupants keeps at a constant level. Thirdly, rather than facilities, occupants release the primary contaminants that affect cross-infection. Fourthly, partitions decrease the airflow in the indoor space, which reduces the risk of cross-infection but also decreases the ventilation effect. Lastly, the energy-saving performance also plays an important role because of the long-term operation.

Impinging jet ventilation (IJV) systems would be a promising alternative in cooling densely occupied spaces. Imping jet diffusers supply cold air with high momentum that impinges on the floor and forms a thin cold air layer [19]. This layer of air can reach far due to high momentum and negative buoyancy. This type of system may remove contaminants more efficiently and consume less energy than traditional MV systems. Wang et al. [20] reported that the IJV system has a higher contaminant removal effectiveness than MV systems in an intensive care unit.

However, there are several research gaps regarding the performances of IJV systems for densely occupied spaces. Firstly, previous research on IJV performances focused primarily on small enclosures or spaces with few rows of occupants. For instance, Qin et al. [19,21] and Ye et al. [22] reported CO_2 distribution in a small office with two staff; Wang et al. [20] investigated the contaminant removal for an intensive care unit occupied by four occupants. Secondly, investigations about IJV systems focused mainly on thermal comfort, IAQ, and energy saving, while IJV system's performance on the risk of cross-infection is rarely studied. For example, thermal stratification was the main focus in Refs. [23,24]. Thirdly, the infectors (the source of virus-laden contaminants) were identified and fixed in previous research (e.g., Ref. [25]). In contrast, it is hard to locate the source of virus-laden contaminants in public spaces because some infected people are asymptomatic. Lastly, previously studied duct diffusers of the IJV system might be insufficient since densely occupied spaces demand high ventilation.

Computational fluid dynamics (CFD) is an efficient tool for ventilation research, as it is time-efficient and reliable when well-validated and has thus become a powerful tool due to the rapid development of computing power. CFD simulations can obtain distributions of parameters, such as temperature, velocity components, and various contaminants in an entire target space [26]. It has been widely used to simulate airflow patterns created by ventilation systems. For instance, Gilani et al. [27] simulated the temperature stratification of a DV system. Wang et al. [20] simulated the exhaled droplet distribution in an intensive care unit. Furthermore, Liu et al. [28] evaluated infection risk in a BSL-3 laboratory via embedding the Wells-Riley model into a CFD model.

This study proposes a modified type of IJV system to cool densely occupied spaces. A classroom is taken as the example to illustrate this IJV system's performance in removing exhaled contaminants, saving energy, and providing a thermally comfortable environment. A traditional MV system is taken as a reference. It is assumed all occupants wear masks in the right way [29] and all of them are healthy or asymptomatic; thus, the released breathing contaminants are small enough [30] and are reliable to be modeled as a tracer gas [31].

2. Models and methods

2.1. Physical model

Current IJV systems generally use duct diffusers (Fig. 1a, see Refs. [23,25,32]), which might be insufficient to meet the large demand of ventilation rate for densely occupied large spaces. A modified IJV system is proposed in this study to cool a large space (11.3 × 7.2 × 5.0 m^3) occupied by 50 occupants (Fig. 1b), i.e., about 1.6 m^2 per occupant [15]. Occupants are simplified as columns with a size of 0.3 × 0.3 × 1.2 m^3. The occupied zone (OZ) is from the floor to the height of 1.8 m and 1.0 m from each vertical wall. The exhaust/return-split layout [33] is employed, and the return vents (2.7 × 0.5 m^2 each) are at the mid-level (2.25 m from the floor in this study) [34] to save energy. Two supply diffusers (2.3 × 0.2 m^2 each) are mounted 0.6 m above the floor [35]. Two exhausts are located at the center of the ceiling with a size of 925 × 700 mm^2 each. Lamps are modeled as surfaces at the ceiling with a size of 9.3 × 0.3 m^2. This study locates occupants symmetrically to the classroom's central plane (x = 5.65 m) to reduce computing costs. An MV system (Fig. 1c) is used as a reference. Its supply diffusers are located near the ceiling, and return vents are near the floor [36,37]. The geometrical differences between the MV system and the modified IJV system (hereafter referred to as IJV system) are the return vents' location and the supply diffusers' direction and location.

2.2. Computational fluid dynamics model for airflows

2.2.1. Governing equations

Navier-Stokes equations in steady-state govern airflows in this study. Thermal buoyancy is critical to forming thermal stratification. It is usually modeled as a source term in the momentum conservation equation via Boussinesq approximation [38,39] or incompressible ideal gas law [40,41]. This study utilizes the incompressible ideal gas law. The radiative heat transfer is modeled by the discrete ordinates method [42]. The CO_2 distribution is governed by the species transport equation [43]. The binary mass diffusion coefficient is determined by the Fuller correlation [44,45]. The flow turbulence is modeled via the shear stress transport (SST) k-ω model [46]. The governing equation for the mean age of air (MAA) [47] is:

$$\rho\frac{\partial \tau u_j}{\partial x_j}=\frac{\partial}{\partial x_j}\left[\left(2.88\rho\times10^{-5}+\frac{\mu_{eff}}{Sc_t}\right)\frac{\partial \tau}{\partial x_j}\right]+\rho \quad (1)$$

where τ is MAA in second, μ_{eff} is the effective viscosity, and Sc_t is the turbulent Schmidt number, 0.7 [48].

2.2.2. Boundary conditions

Heat flux per manikin is 76 W (i.e., 1.0 met) [49]; thus, the heat flux boundary condition is approximately 50 W/m^2. The light power is 10 W/m^2 for the room [50], i.e., 813.6 W for the entire room. The lamps' heat flux is 58.3 W/m^2 to meet the requirement of the light power because the lamps' area is 13.95 m^2 (Fig. 1). Previous research used various types of thermal boundaries to model vertical walls. For instance, Shokrollahi et al. [14] assumed vertical wall insulation, Fan et al. [34] modeled vertical wall heat transfer via heat transfer coefficient and outdoor air temperature, and Ye et al. [22] converted the heat transfer coefficient and outdoor temperature into a given heat flux. This study assumes a fixed heat flux of 12.5 W/m^2 for vertical walls following ref. [22]. Fresh air for each occupant is 24 m^3/h for classrooms [51], i.e., 0.4 kg/s for the entire space with 50 students. Supply velocity (consisting of fresh air and returned air) is 1.0 m/s, i.e., 0.92 m^3/s for the entire room. The turbulent intensity at supply diffusers is calculated following Eq. (2):

$$T_u=0.16\,Re^{-0.125} \quad (2)$$

where Re is the Reynolds number calculated based on the length scale of

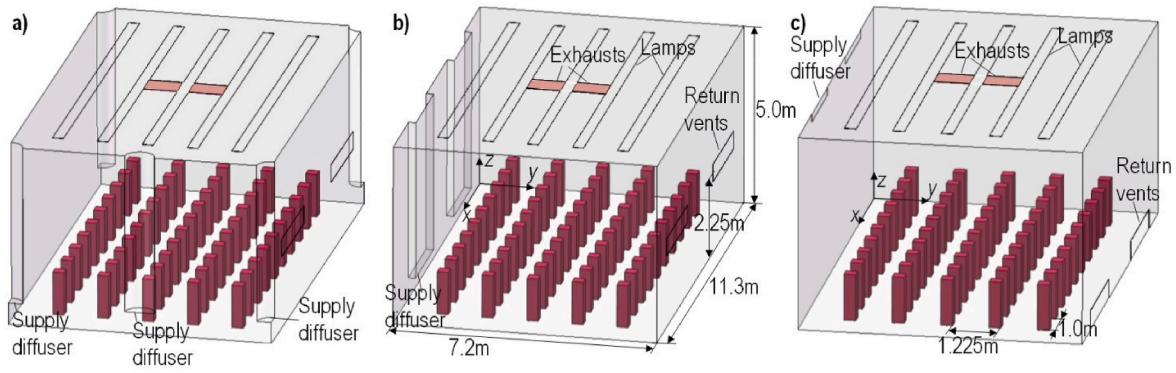

Fig. 1. The physical model of a densely occupied space cooled by a) an IJV system (merely serves as an example and is not investigated in this paper), b) a modified IJV system, and c) an MV system.

$0.07 \times d_h$, d_h is supply diffuser's hydraulic diameter. Carbone dioxide mass fraction at the supply diffuser is determined by mixing the return air and fresh air [22], which is calculated via the following equation:

$$S_s = \frac{S_r \dot{m}_r + S_f \dot{m}_f}{\dot{m}_s} \tag{3}$$

where S_s, S_r, and S_f are the species mass fraction at the supply diffuser, return vent, and fresh air, respectively, and $\dot{m}_f$, $\dot{m}_r$, and $\dot{m}_s$ are the fresh air flow rate, the return air flow rate, and the supply air flow rate, respectively. Breathing jets are significantly weakened by the face mask, and most of them are entrained into the body plume [1]. Therefore, the occupant-generated CO_2 is released in front of each manikin face above the floor 1.1 m. ASHRAE Standard [52] describes that the CO_2 generation rate is 0.31 L/min. Carbon-dioxide density is 1.951 g/L under an air pressure of 1 bar and an air temperature of 0 °C. Therefore, the generation rate is ~0.01 g/s. The surgical mask filters particles larger than 0.1 μm with >98% efficiency [30]. Thus, the exhaled virus-laden aerosols are modeled as tracer gas released in front of each manikin. The tracer gas can be CO_2 or SF_6; this study uses CO_2 and calls it tracer gas to differ from CO_2. The tracer gas at the supply diffusers is zero, i.e., the returned air is disinfected thoroughly. Table 1 summarizes the boundary conditions for the simulations for both the modified IJV system and the MV system.

2.2.3. Solution schemes and convergence criteria

ANSYS Fluent 19.2 [48] is used to solve the CFD model. The velocity field is coupled with the pressure field via SIMPLEC algorithm. Convection terms are discretized by the QUICK scheme. The solution is taken as converged when: a) scaled residuals do not drop with further iterations or residuals of the continuity equation and the energy equation drop to 1×10^{-3} and 1×10^{-6}, respectively, and b) simultaneously, the monitored temperature oscillates within a tolerance of 0.1 K in respect to iteration.

Table 1
Boundary conditions.

Boundaries	Conditions
Floor/Ceiling	Adiabatic
Vertical walls	12.5 W/m^2
Lamps	58.3 W/m^2
Manikin	50 W/m^2
Supply diffuser	1.0 m/s, supply temperature is variable to achieve a thermoneutral environment
Exhaust	0.2 kg/s for each exhaust
Return vent	Pressure outlet
CO_2 source/tracer gas source	0.01 g/s
Outdoor	30.8 °C [51]

2.2.4. Model validation

The CFD model is validated by comparing simulated velocity along the jet centerline (Fig. 2b) with velocity measured by Han and Li [53] in a room ($7.0 \times 5.4 \times 3.16$ m^3) with a wall-attached jet supply (Fig. 2a). The supply diffuser and exhaust sizes are 2.0×0.05 m^2 and 0.4×0.2 m^2, respectively. Details of the experiment can be found in Ref. [53]. The supply velocity, u_0, is 1.0 m/s. The comparison between simulated velocity distributions and measured counterparts (Fig. 2c–d) shows that the centerline velocity (i.e., $u_{m,x}$ and $u_{m,y}$) is simulated accurately. Therefore, the CFD model is validated.

Additionally, the experiment in Ref. [53] was conducted under an isothermal situation. Validation of the heat transfer and thermal buoyancy models can be found in our previous research [54,55]. The simulated velocity, temperature, and turbulent kinetic energy were compared with measured data reported by Kobayashi et al. [23]. Another of our previous research [45] validated the species transport model by comparing the simulated contaminant concentration released from a surface in a virtual wind tunnel with the measured concentration reported by Saha et al. [56].

2.2.5. Grid independence test

To eliminate the impacts of grids on simulated results, this study refines the grid (via ANSYS ICEM) till the finer grid does not change the simulated results anymore. The MV and IJV systems (see Fig. 1) are both tested. Only grids and results of the room with the IJV system are presented (Fig. 3) to illustrate the grid test procedure, and the room with the MV system is tested in a similar way. For the IJV system, three grids (Fig. 3a–c) are tested, i.e., the coarse (1,213,267 cells), the medium (2,948,428 cells), and the fine (5,562,778 cells). Grids in the wall vicinity are refined to meet the requirement of the SST k-ω model, i.e., the first layer of cells should be located within the viscous sublayer ($y^+ < 5$). Generally, y^+ is recommended to be around one. Fig. 3d shows the contour of y^+, in which most y^+ of first layer cells are near 1, indicating the grids are fine enough in the wall vicinity. Temperatures along three lines in an aisle (Fig. 3e) are compared among various grids. Fig. 3f–h shows that differences resulting from these grids are limited. Quantitatively, the grid convergence index (GCI) [57] value is less than 5% (see Table 2), indicating these three grids are fine enough. This study selects the medium one because the coarse one is hard to converge during iteration.

2.3. Evaluation indices

2.3.1. Indoor air quality

This study evaluates IAQ via MAA in the OZ, CO_2 in the OZ, and CO_2 in the breathing zone. Regions with longer MAA indicate poor ventilation because the supplied air is difficult to reach [32,58]. The transport of CO_2 in the ventilated enclosure is reliable for representing the

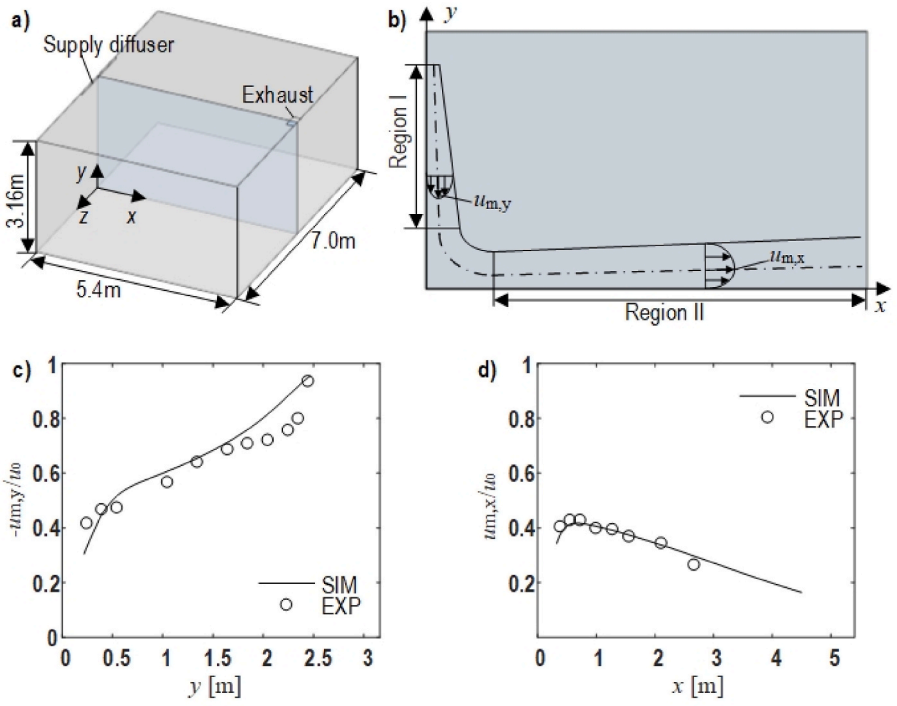

Fig. 2. Model validation: a) the tested room with a wall-attached jet supply; b) the schematic of the velocity along the jet centerline on the central plane; c) and d) the simulated velocity and experimentally measured velocity in the region I and region II, respectively. $u_{m,x}$ and $u_{m,y}$ are the maximum velocity at the section in the region.

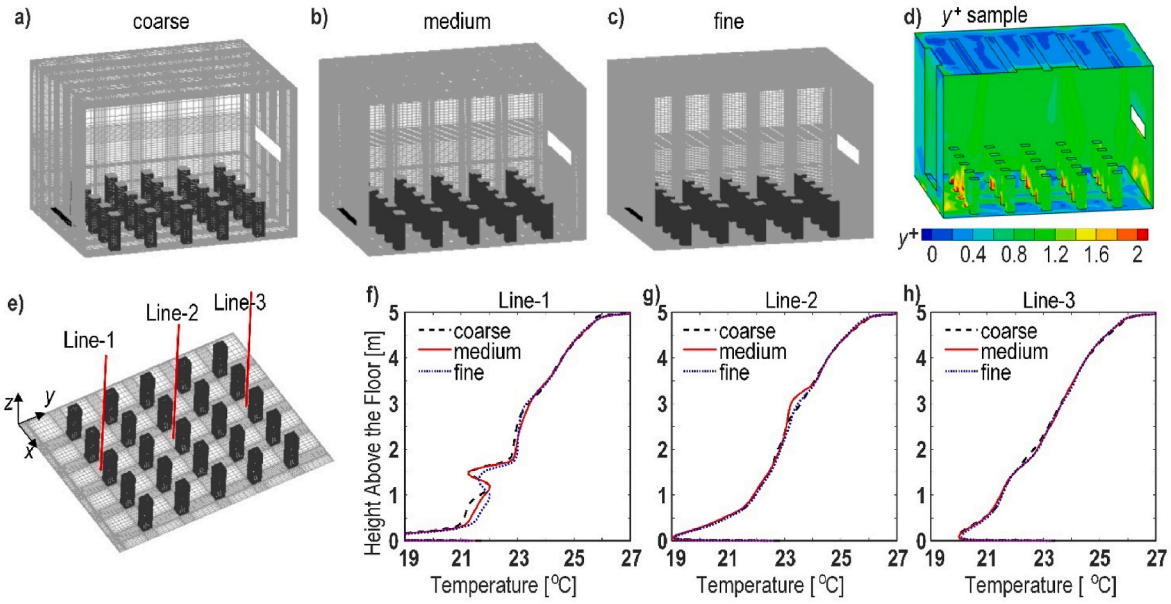

Fig. 3. Grid independence test for the IJV system: a-c) coarse, medium, and fine grids, d) an example of y^+ distribution, e) location of lines for comparison between different grids, f-h) temperature along Lines 1–3 simulated based on coarse, medium, and fine grids.

transport of human-released pollutants [31]. Semi-volatile organic compounds [59] and suspended particles [60,61] obey transport equations like the species transport equation [62]. As reported, the measured variation of total volatile organic compounds regarding time is similar to that of CO_2 in a classroom [63]. Additionally, the exposure index, evaluating the cross-infection risk, is defined as the ratio of inhaled CO_2 concentration over the ambient CO_2 concentration [17].

2.3.2. Infection probability

The infection probability P is calculated following Wells-Riley model [64], which introduces the concept of quanta as the dose of pathogens causing infection [6,28]. It is expressed as Eq. (4):

$$P = 1 - e^{-n_{quantum}} = 1 - e^{-\frac{Iqptv}{Q}} \quad (4)$$

where $n_{quantum}$ is the inhaled infectious quanta, p is pulmonary ventilation rate, t is the exposure time, I is the number of infectors, Q is the

Table 2
GCI values based on temperature.

	IJV			MV		
	Line-1	Line-2	Line-3	Line-1	Line-2	Line-3
GCI_{mc}[a] [%]	0.06	0.16	0.13	0.02	0.05	0.03
GCI_{fm} [%]	0.07	0.22	0.26	0.78	3.44	4.20

[a] The subscripts c, m, and f denote the coarse, medium, and fine grid, respectively.

ventilation rate for the room, V is the room volume.

Considering perfect mixing rarely exists [65], the Wells-Riley model is modified [66] as follows:

$$P = 1 - e^{-tpE} \tag{5}$$

where E is the inhaled quanta concentration.

This study uses tracer gas (i.e., CO_2) to represent virus-laden aerosols. A unit mass of CO_2 corresponds to the number of quanta calculated following Eq. (6):

$$q_{CO2} = \frac{q}{Q_{CO2}} \tag{6}$$

where Q_{CO2} is the generation rate of the tracer gas for each infector, q is the quanta generation rate.

The local infection-risk based on tracer gas is as follows:

$$P = 1 - e^{-\theta t p S_{CO2} q_{CO2}} = 1 - e^{-\theta t p S_{CO2} q / Q_{CO2}} \tag{7}$$

where S_{CO2} is the local mass concentration of the tracer gas from CFD results, θ is the permeability coefficient of masks (0.05 [28]). The parameters to calculate P in this study are listed in Table 3. It is noteworthy that the infection probability in this study is for the relative magnitude of virus-laden aerosol concentration [67]. The tracer gas (CO_2) distribution for infection probability is simulated when only the infector releases CO_2 and no CO_2 in the supply diffuser (i.e., no virus in returned air and fresh air).

Inhaled contaminant intensity is usually modeled as a mass fraction at the breathing zone [69], generally a small cubic or sphere space near the nose or mouth [69,70]. This study uses the average contaminant mass fraction in the space surrounding the head as an alternative. The head region [71] is assumed as a cubic space surrounding the target manikin with a thickness of 0.1 m [72] from 0.9 m to 1.3 m above the floor (Fig. 4).

2.3.3. Nonuniformity

The thermal environment for several occupants is non-uniform in horizontal planes [73], which might induce discomfort in certain areas, although the average thermal environment is acceptable. Zhang et al. [74] proposed velocity nonuniformity index (VNI) and temperature nonuniformity index (TNI) to evaluate the nonuniformity. Accordingly, in this study, the VNI is defined, at both the ankle and the head levels, as below:

$$\mathrm{VNI} = \frac{\sigma_U}{\overline{U}}, \sigma_U = \sqrt{\frac{\sum A_i (\overline{U}_i - \overline{U})^2}{A}} \tag{8}$$

where $\overline{U}_i$ is the area-averaged velocity magnitude at the ith discretized facet in the target plane, A_i is the area of the ith facet, $\overline{U}$ is the area-averaged velocity magnitude at the entire plane, and A is the overall area. However, the ANSYS Fluent does not store the face area for internal slices. This study replaces the facet area A_i and the entire area A with the cell volume V_i and the volume V of a thin layer of cells at the corresponding level in postprocessing.

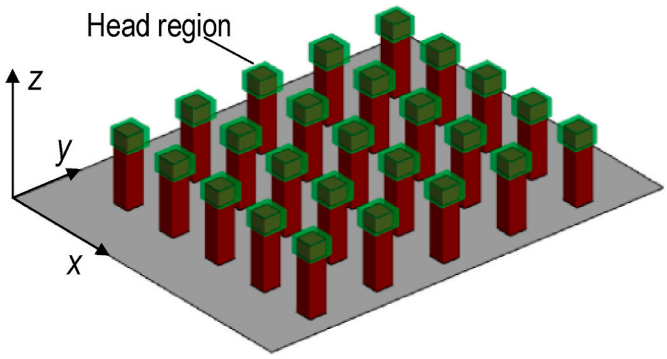

Fig. 4. Head regions (i.e., a cubic around the head of each manikin).

Similarly, TNI at the ankle level and head level is defined as:

$$\mathrm{TNI} = \frac{\sigma_T}{\overline{T}}, \sigma_T = \sqrt{\frac{\sum A_i (\overline{T}_i - \overline{T})^2}{A}} \tag{9}$$

where $\overline{T}_i$ is the area-averaged temperature at the ith facet, and $\overline{T}$ is the area-averaged temperature at the entire plane.

In particular and more importantly, regarding the exhaled air distribution, a new assessment formula, the species nonuniformity index (SNI) of CO_2 at the head level is proposed and expressed by Eq. (10) listed below:

$$\mathrm{SNI} = \frac{\sigma_S}{\overline{S}}, \sigma_S = \sqrt{\frac{\sum A_i (\overline{S}_i - \overline{S})^2}{A}} \tag{10}$$

where $\overline{S}_i$ is the area-averaged CO_2 mass fraction at the ith facet, $\overline{S}$ is the area-averaged mass fraction at the entire plane.

2.3.4. Energy consumption

Cooling coil load, Q_{coil}, is used to evaluate the energy consumption performance of the system. For a system with the exhaust/return-split layout (Fig. 5), Q_{coil} is calculated by the following equation [75,76]:

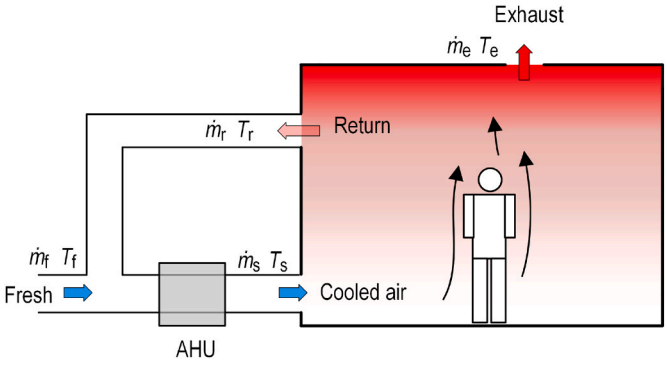

Fig. 5. Scheme of a system with exhaust/return-split layout. AHU is the air-handling unit.

Table 3
Parameters to calculate infection probability P.

t [h]	θ [−]	p [m^3/h]	S_{CO2} [kg/m^3]	Q_{CO2} [kg/h]	q [quanta/h]
1 [68]	0.05 [28]	1.222 [28]	From CFD	0.036 (i.e., 0.01 g/s)	10.5 [25]

$$Q_{coil} = Q_{space} - c_p \dot{m}_f (T_e - T_f) \quad (11)$$

where Q_{spcae} is the space cooling load (consisting of heat sources and external heat flux through walls), T_e is the exhaust temperature, and T_f is the fresh air temperature. The fresh air flow rate $\dot{m}_f$ equals the exhaust flow rate $\dot{m}_e$ for airtight spaces.

2.3.5. Thermal comfort

Predictive mean vote (PMV) is used to evaluate the thermal comfort performance of the ventilation system. Local PMV value is calculated via Fanger's model [77,78] based on the simulated variables (e.g., velocity, temperature, and mean radiant temperature). In this study, the metabolic rate is 58 W/m^2 (1.0 met), mechanical work is zero, the thermal resistance of clothing is 0.089 m^2 K/W, and ambient relative humidity is 60% [73]. The threshold of $|PMV| < 0.5$ is suggested for general thermal comfort [78].

The temperature difference between the head and ankles is calculated by the following equation:

$$\Delta T_{0.1-1.1} = T_{1.1} - T_{0.1} \quad (12)$$

where $T_{0.1}$ and $T_{1.1}$ are average temperatures at $z = 0.1$ m and $z = 1.1$ m, respectively. The acceptable temperature difference is 3 °C [79].

2.4. The procedure to achieve thermoneutral occupied zone

Demand-controlled systems are emerging, of which the indoor temperature can be tuned to obtain a thermally comfortable environment and simultaneously save energy [9,80,81]. This study tuned the supply temperature to achieve a thermoneutral environment inside the OZ. The trial starts from an initial supply temperature of 18 °C, which results in OZ-averaged PMVs lower than −0.5, i.e., the OZ is overcooled. A series temperature interim (i.e., 19–25 °C) follows. The final supply temperature for both MV and IJV systems is finalized as the one leading to the OZ environment satisfying $|PMV|<0.5$ and the PMV as close to zero as possible. Hence, as shown in Fig. 6, the final supply temperatures for the MV and IJV systems are chosen as $T_s = 22$ °C and 24 °C, respectively.

3. Results and discussions

This study compares the performances of the newly modified IJV system with a traditional MV system. Contours in several key planes are shown to demonstrate the feature of velocity, temperature, and IAQ. These planes are visualized in Fig. 7.

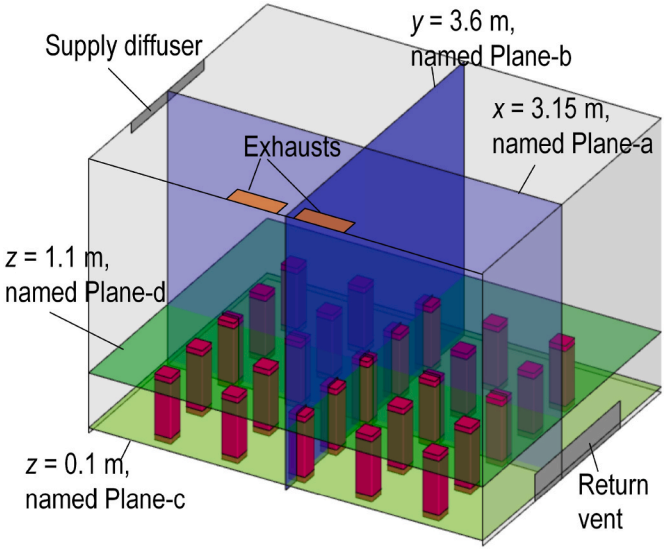

Fig. 7. Selected planes for outputs demonstration of both ventilation systems.

3.1. Velocity fields

The velocity distribution is shown in Fig. 8. For the MV system, the cooled air jets through the diffuser and then flow downwards due to the buoyancy effects (Fig. 8a–b), consistent with the velocity distribution for an MV system reported by Zhong et al. [82]. The downward airflow eventually impinges onto the floor and spreads out (Fig. 8c). For the IJV system, the supplied air impinges onto the floor and flows upward when it encounters manikins (Fig. 8e). At the ankle level (i.e., $z = 0.1$ m), impinged air spreads mainly along aisles between occupants and forms branches when encountering manikins (Fig. 8f–g). The branches might be caused by the expansion of the jet flow in aisles and the interference between the airflow and manikins.

Velocity distributions at the ankle level ($z = 0.1$ m) and the head level ($z = 1.1$ m) show that the IJV system leads to a less uniform velocity than the MV system at the ankle level, while a more uniform velocity at the head level (Fig. 8c–d & 8g-8h). Quantitatively, the VNI at the ankle level, $VNI_{0.1}$, increases from 0.54 to 0.96 (Table 4). At the head level, the standard deviation of temperature, $\sigma_{U,1.1}$, drops from 0.12 m/s to 0.05 m/s though $VNI_{1.1}$ increases a bit (Table 4), indicating a more

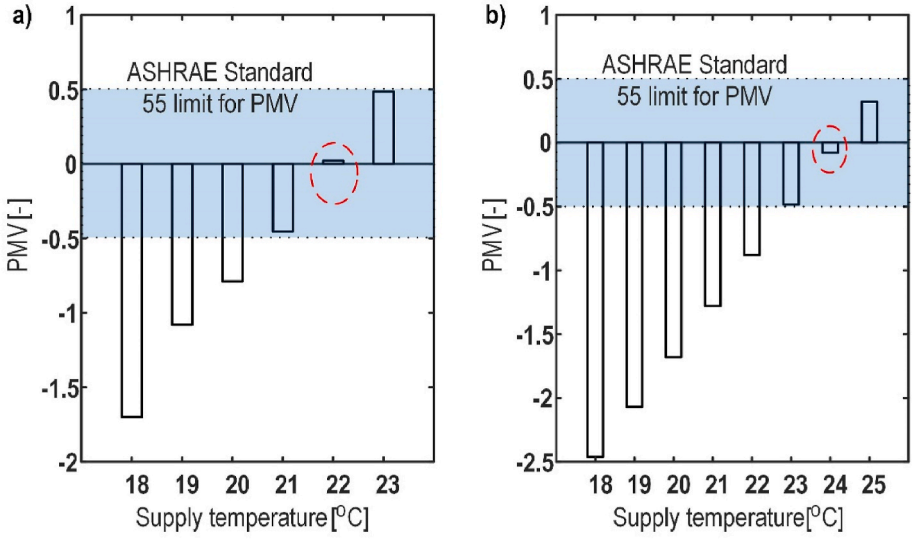

Fig. 6. PMVs in the OZ under various supply temperatures for a) the MV system and b) the IJV system.

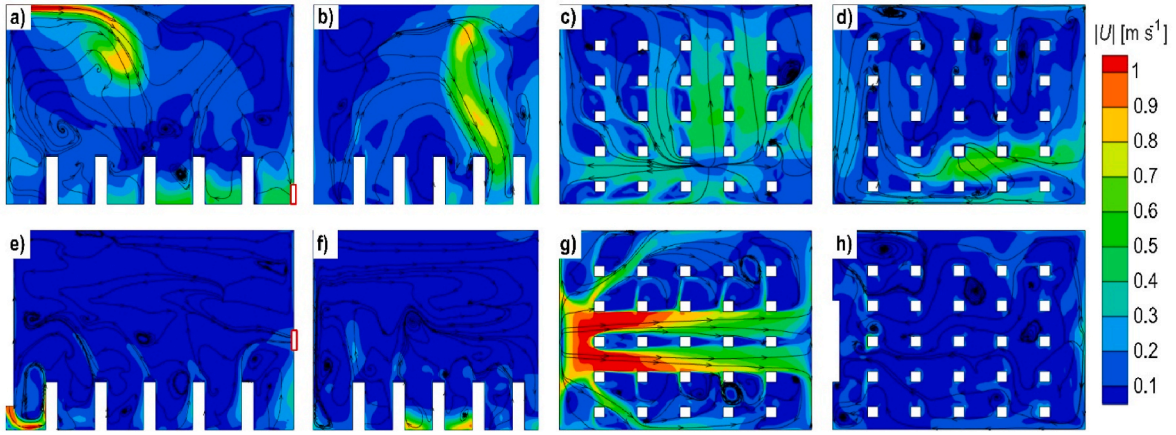

Fig. 8. Velocity contours a-d) of the MV system at Planes-a, b, c, & d, respectively, and e-h) of the IJV system at Planes-a, b, c, & d, respectively. Red squares mark the return vent location. (For interpretation of the references to colour in this figure legend, the reader is referred to the Web version of this article.)

Table 4
Nonuniformity indexes at the ankle and head levels.

	U at ankle		*U* at head		*T* at ankle		*T* at head		CO_2 at head	
	$VNI_{0.1}$ [-]	$\sigma_{U,0.1}$ [m/s]	$VNI_{1.1}$ [-]	$\sigma_{U,1.1}$ [m/s]	$TNI_{0.1}$ [-]	$\sigma_{T,0.1}$ [K]	$TNI_{1.1}$ [-]	$\sigma_{T,1.1}$ [K]	$SNI_{1.1}$ [-]	$\sigma_{S,1.1}$ [ppm]
MV	0.54	0.13	0.61	0.12	0.0024	0.71	0.0022	0.67	0.28	375.7
IJV	0.96	0.30	0.71	0.05	0.0041	1.24	0.0021	0.63	0.38	427.4

uniform velocity distribution.

3.2. Temperature fields and thermal comfort performances

The temperature contours of MV and IJV systems are demonstrated in Fig. 9. When the MV system is used, the cold air is supplied near the ceiling and then cools the room via mixing (Fig. 9a–b). Temperature distributions at the ankle and head levels are relatively uniform (Fig. 9c–d), which indicates that the indoor air is well mixed. When the IJV system is used, thermal stratifications in the classroom can be observed along the vertical direction (Fig. 9e–f), indicating the satisfactory operation of the system. At the ankle level, the IJV system degrades the uniformity of temperature (Fig. 9c–g, Table 4). Meanwhile, the temperature uniformity at the head level remains almost unchanged (Fig. 9d–h, Table 4). Summarily, the MV system produces more uniform temperature distributions than the IJV system.

The temperature differences between the head and ankles are calculated using Eq. (12) at the level of 0.05 °C and 1.34 °C for the MV system and IJV system (Table 5), respectively. In other words, the IJV system enlarges the vertical temperature gradient between the head and ankles. On the other hand, both systems meet the requirement of vertical temperature gradient for an acceptable environment ($\Delta T_{0.1\text{-}1.1}$<3 °C).

Distributions of local PMV are presented in Fig. 10. The overcooled region (i.e., PMV < −0.5) mainly locates in the upper part of the room under the MV system (Fig. 10a–b). In the OZ, the overcooled region is observed (circled in Fig. 10c–d) due to the downward airflow. Under the IJV system, the upper part of the room is left uncooled while the OZ is cooled well (Fig. 10e–f). At the ankle level (Fig. 10g), a large area along the pathway of the jet flow is overcooled, which is consistent with the

Table 5
Performances of the ventilation systems in IAQ and energy consumption.

	MAA [s]	CO_2 [ppm]	PMV [−]	Q_{coil} [W]	T_e [K]	$\Delta T_{0.1\text{-}1.1}$ [°C]
MV	439	1287	0.02	7762	28.7	0.05
IJV	177	1078	−0.08	6148	32.1	1.34

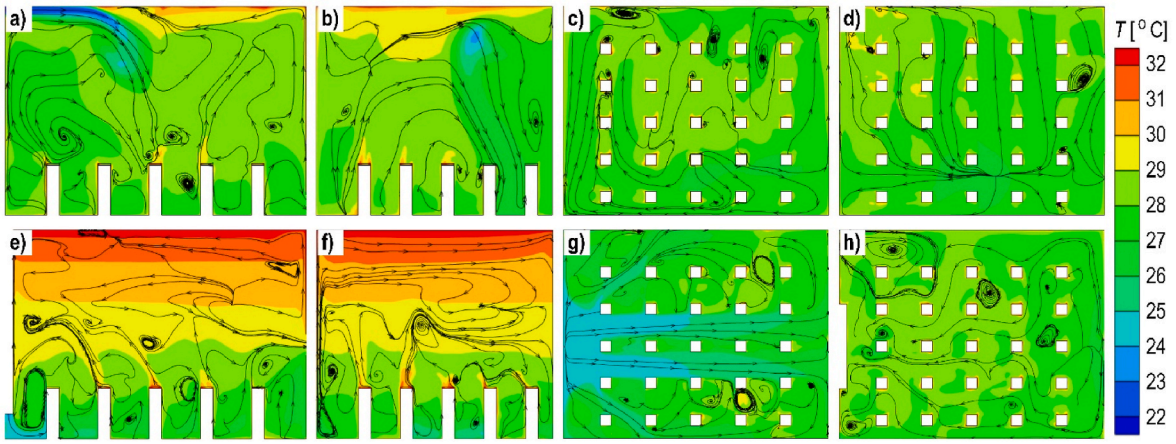

Fig. 9. Temperature distribution a-d) of the MV system at Planes-a, b, c, & d, respectively, and e-h) of the IJV system at Planes-a, b, c, & d, respectively.

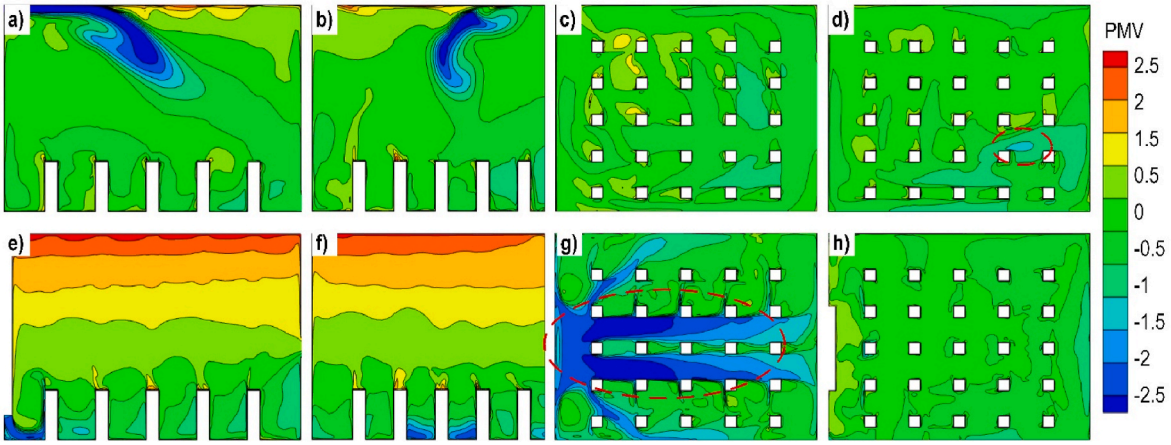

Fig. 10. PMV distributions a-d) of the MV system at Planes-a, b, c, & d, respectively, and e-h) of the IJV system at Planes-a, b, c, & d, respectively.

velocity and temperature fields. At the head level (Fig. 10h), most of the area is thermally comfortable (i.e., $|PMV|<0.5$), indicating the well-cooling of the head region with the IJV system.

3.3. Indoor air quality

IAQ is gauged via CO_2 concentration and MAA, particularly at the breathing level. The CO_2 distribution is shown in Fig. 11. Generally, CO_2 spreads upward due to the thermal plumes of manikins, which is consistent with previous research [46,61]. The indoor air is well mixed for the MV system; consequently, the CO_2 concentration created by the MV system is more uniform than that created by the IJV system. On the other hand, the MV system results in a higher concentration of CO_2 in the OZ than the IJV system. At the head level (i.e., $z = 1.1$ m), the CO_2 concentration is significantly reduced by the IJV system (Fig. 11c and f). The nonuniformity index and the standard deviation (see $SNI_{1,1}$ and $\sigma_{S,1,1}$ in Table 4) of the IJV system is higher than that of the MV system. Therefore, the MV leads to a more uniformly distributed CO_2 at the head level. For the IJV system, the CO_2 in the diffuser vicinity (Fig. 11f) is higher than in the region away from the diffuser, which may be caused by the recirculation airflow (marked by dashed arrows in Fig. 11d).

The MAA at the head level (Fig. 12) shows that the IJV system leads to a much lower MAA than the MV system. Quantitatively, the MAA in the OZ is shortened from 439 s to 177 s (Table 5). Summarily, the IJV system highly improves IAQ in the OZ.

3.4. Cross-infection risk

It is unknown whether one is infected or not in public indoor spaces until the syndrome of infectors is obvious. To evaluate the performances in cross-infection, this study locates the infector as the manikin owning the highest potential to transmit his/her tracer gas elsewhere. The tracer gas distribution (Fig. 13a & b) is obtained under the condition that all manikins release tracer gas. The lowest tracer gas concentration in the head region is at the position of Manikin-2 for the MV system and at the position of Manikin-1 for the IJV system (Fig. 13a & b).

The infection probability is shown in Fig. 14. The highest risk for the IJV system is a bit higher than that for the MV system, while the mean risk of all occupants is lower. The average infection probability is reduced from 0.047% to 0.027% when the infector is Manikin-1 and from 0.035% to 0.024% when the infector is Manikin-2. For the IJV system, the highest risk position is near the supply diffuser, which agrees with the airflow field that thermal plumes flow upward and emerge into the recirculation airflow (Fig. 11d). Contaminants are accumulated near the diffuser due to the recirculation airflow. These high-risk positions partly coincide with the overcooled region marked in Fig. 10g,

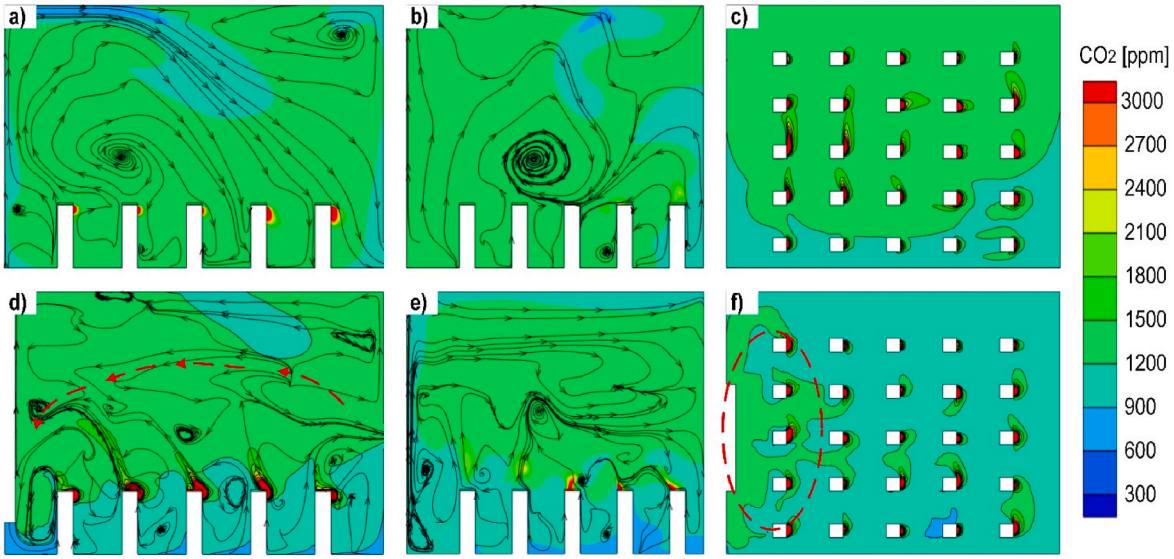

Fig. 11. Carbon-dioxide distribution a-c) of the MV system at Planes-a, b, & d, respectively, d-f) of the IJV system at Planes-a, b, & d, respectively.

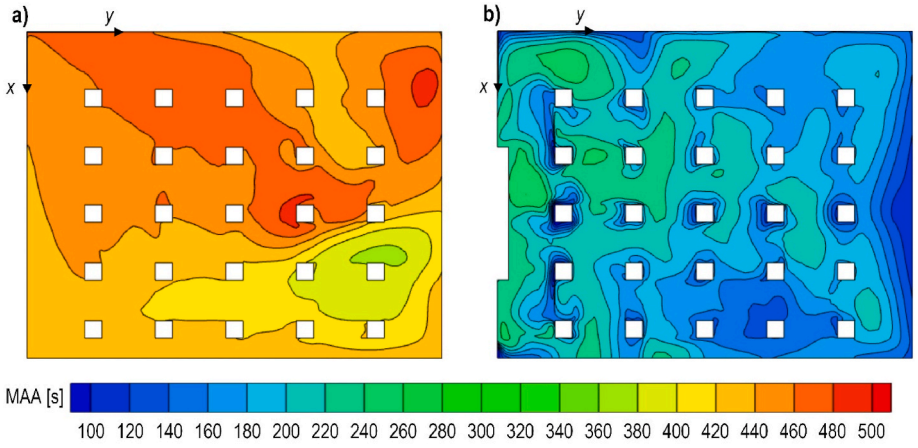

Fig. 12. MAA at the breathing level ($z = 1.1$ m) for the a) MV and b) IJV systems.

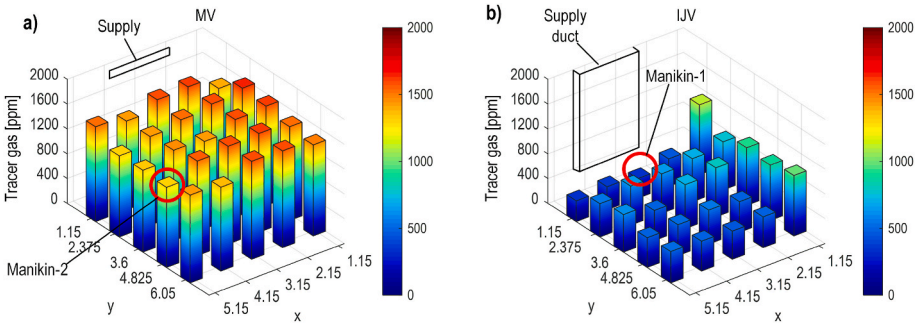

Fig. 13. The tracer gas mass fraction in the head region when the supplied air is disinfected for a) the MV system and b) the IJV system.

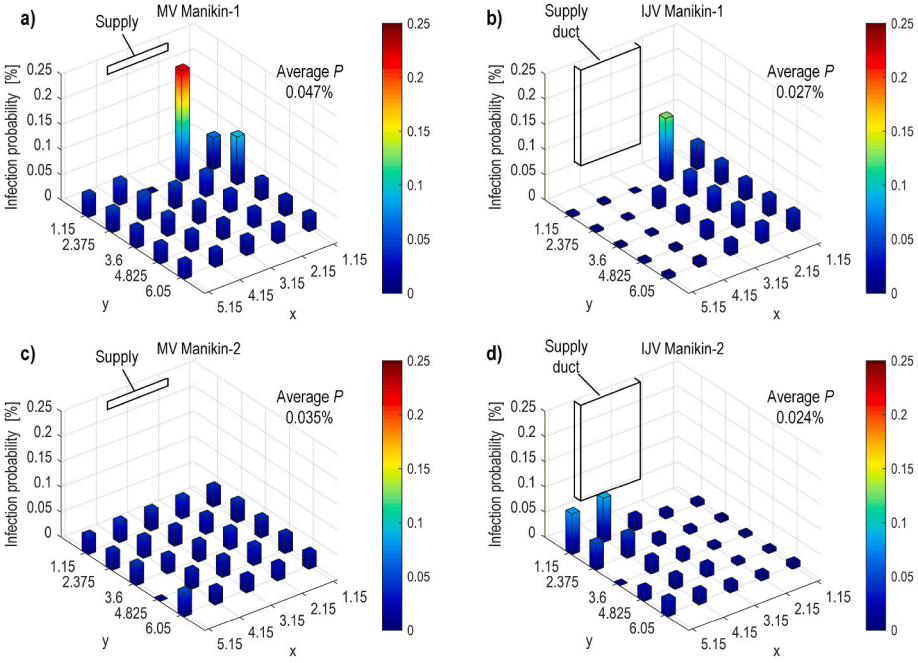

Fig. 14. Infection probability of each manikin a-b) for assuming Manikin-1 as the infector, and c-d) for assuming Manikin-2 as the infector.

indicating that a larger margin between the supply and OZ might improve thermal comfort performance and reduce cross-infection risk simultaneously.

3.5. Cooling coil load

In this study, the energy consumption of cooling systems is evaluated by cooling coil load, Q_{coil} (calculated by Eq. (11)). The IJV system

reduces Q_{coil} from 7762 W to 6148 W (Table 5), i.e., a reduction of 20.8%. The decrease of Q_{coil} is because a) the IJV system cools OZ and leaves upper space uncooled, b) a higher supply temperature can be used, and c) the exhaust temperature in the IJV system is higher than that in the MV system (Table 5), i.e., the wasted cooling load is reduced.

3.6. Limitations

There are several limitations to this study, despite the effectiveness of the modified IJV system in mitigating exhaled contaminants and saving energy. Firstly, the energy consumption is evaluated via cooling coil load, while a higher supply temperature means lower demands for exergy (e.g., a higher coefficient of performance of chillers [83,84]) to cool the returned and fresh air [85]. Therefore, the energy-saving performance will be more significant if the energy conversion efficiency is considered. Secondly, the IJV system performs better than the MV system in IAQ and energy saving but worse in thermal comfort. The IAQ is suggested to have a higher priority than thermal comfort due to the high basic reproduction number of COVID-19, and the thermal comfort may be adaptive due to personal conditions [86,87], e.g., the difference in clothes. This content will be further optimized. Thirdly, the infection probability is for the relative magnitude of risk. The quantum to cause infection [88] and its effects on infection probability need to be further investigated.

4. Conclusions

The pandemic of COVID-19 has been raising much attention on IAQ. This study proposes a modified IJV system to cool a densely occupied space in which all occupants wear masks, and it is unknown whether they are infected or not. The infector is assumed as the manikin owning the highest potential to transmit his/her tracer gas elsewhere, i.e., the one with the lowest tracer gas mass fraction in the head region. The manikin with the lowest tracer gas concentration under the IJV and MV systems are named Manikin-1 and Manikin-2, respectively. The Occupants are assumed to release CO_2 and virus-laden tracer gas at a given rate. The performance of the IJV system is compared with a traditional MV system.

The main results can be drawn as below.

a) The IJV system leads to higher IAQ and simultaneously consumes less energy than the MV system. The OZ-averaged CO_2 concentration is reduced from 1287 ppm to 1078 ppm, and the OZ-averaged MAA drops from 439s to 177s. The mean infection probability is reduced from 0.047% to 0.027% when the infector is Manikin-1 and from 0.035% to 0.024% when the infector is Manikin-2. The cooling coil load is reduced from 7588 W to 6148 W.
b) However, the IJV system leads to a less uniformly distributed temperature, velocity, and CO_2. The vertical temperature difference ($\Delta T_{0.1\text{-}1.1}$) increases from 0.05 °C to 1.34 °C, and the region near the supply at the ankle level is overcooled. The VNI at the head level increases from 0.54 to 0.96, and of CO_2 mass fraction increases from 0.28 to 0.38.

Summarily, the modified IJV system effectively removes exhaled contaminants in densely occupied spaces and simultaneously consumes less energy than traditional MV systems, indicating that the IJV system performs well in cooling and ventilating densely occupied spaces. However, this system might induce overcooling at the ankle level. Thus, further studies to improve nonuniformity are suggested.

The study verifies the advantages (i.e., higher IAQ, lower infection probability, and lower energy consumption) of the IJV system over the MV system in cooling and ventilating densely occupied spaces and reveals the disadvantages (i.e., degradations of thermal comfort and uniformity) of the IJV system. Its conclusions offer a basis and direction for further investigations of the IJV system.

Nomenclature

P	[−] infection probability
p	[m^3/h] pulmonary ventilation rate
q	[quanta/h] quanta generation rate
Q_{coil}	[W] cooling coil load
Q_{space}	[W] space cooling load
Re	[−] Reynolds number
t	[h] exposure time
t_a	[°C] average air temperature

Funding

The work was partially supported by Strategic Research Grants (PJ# 7005679, 7005564), City University of Hong Kong, Hong Kong SAR.

Consent for publication

All authors consent for publication.

Ethics approval and consent to participate

Not applicable.

Availability of data and materials

All data generated or analyzed during this study are included in this manuscript.

CRediT authorship contribution statement

Chao Qin: Writing – original draft, Investigation, Conceptualization. **Shu-Zhen Zhang:** Data curation. **Zheng-Tong Li:** Formal analysis. **Chih-Yung Wen:** Writing – review & editing. **Wei-Zhen Lu:** Writing – review & editing, Supervision, Project administration.

Declaration of competing interest

The authors declare that they have no known competing financial interests or personal relationships that could have appeared to influence the work reported in this paper.

Data availability

The data that has been used is confidential.

Acknowledgments

Not applicable.

t_{cl}	[°C] clothing surface temperature
$\overline{t_r}$	[°C] mean radiant temperature
T_e	[°C] exhaust temperature
T_f	[°C] fresh air temperature
T_s	[°C] supply temperature
$\Delta T_{0.1\text{-}1.1}$	[°C] temperature difference between the head and ankles
u_i	[m/s] the ith component of velocity
$\|U\|$	[m/s] the velocity magnitude
x, y, z	[m] Cartesian coordinates
y^+	[−] nondimensional distance from the cell centers of the first layer grid to the wall

Greek symbols

ρ	[kg/m^3] air density
θ	[−] permeability coefficient of face mask
ν	[m^2/s] kinematic viscosity of air

Abbreviations

IAQ	indoor air quality
IJV	impinging jet ventilation
MV	mixing ventilation
PMV	predictive mean vote
MAA	mean age of air
TNI	temperature nonuniformity index
OZ	occupied zone
SV	stratum ventilation
VNI	velocity nonuniformity index
SNI	species nonuniformity index
CFD	computational fluid dynamics

References

[1] R.K. Bhagat, M.S. Davies Wykes, S.B. Dalziel, P.F. Linden, Effects of ventilation on the indoor spread of COVID-19, J. Fluid Mech. 903 (2020), https://doi.org/10.1017/jfm.2020.720.

[2] Y. Li, H. Qian, J. Hang, X. Chen, L. Hong, P. Liang, et al., Evidence for probable aerosol transmission of SARS-CoV-2 in a poorly ventilated restaurant, medRxiv (2020) 1–19, https://doi.org/10.1101/2020.04.16.20067728.

[3] T.K. Burki, Omicron variant and booster COVID-19 vaccines, Lancet Respir. Med. 10 (2022) e17, https://doi.org/10.1016/S2213-2600(21)00559-2.

[4] E. Ding, D. Zhang, P.M. Bluyssen, Ventilation regimes of school classrooms against airborne transmission of infectious respiratory droplets: a review, Build. Environ. 207 (2022), 108484, https://doi.org/10.1016/j.buildenv.2021.108484.

[5] N.A. Megahed, E.M. Ghoneim, Indoor Air Quality: rethinking rules of building design strategies in post-pandemic architecture, Environ. Res. 193 (2021), 110471, https://doi.org/10.1016/j.envres.2020.110471.

[6] C.C. Wang, K.A. Prather, J. Sznitman, J.L. Jimenez, S.S. Lakdawala, Z. Tufekci, et al., Airborne transmission of respiratory viruses, Science (2021) 373, https://doi.org/10.1126/science.abd9149, 80-.

[7] T. Mikeska, J. Fan, Full scale measurements and CFD simulations of diffuse ceiling inlet for ventilation and cooling of densely occupied rooms, Energy Build. 107 (2015) 59–67.

[8] T. Mikeska, J. Fan, S. Svendsen, Full scale measurements and CFD investigations of a wall radiant cooling system integrated in thin concrete walls, Energy Build. 139 (2017) 242–253, https://doi.org/10.1016/j.enbuild.2017.01.033.

[9] A. Alaidroos, A. Almaimani, M. Krarti, A. Dahlan, R. Maddah, Evaluation of the performance of demand control ventilation system for school buildings located in the hot climate of Saudi Arabia, Build. Simulat. (2021), https://doi.org/10.1007/s12273-021-0854-z.

[10] J. Shen, M. Kong, B. Dong, M.J. Birnkrant, J. Zhang, Airborne transmission of SARS-CoV-2 in indoor environments: a comprehensive review, Sci. Technol. Built. Environ. 27 (2021) 1331–1367, https://doi.org/10.1080/23744731.2021.1977693.

[11] Y. Wang, F. Zhao, J. Kuckelkorn, D. Liu, J. Liu, J. Zhang, Classroom energy efficiency and air environment with displacement natural ventilation in a passive public school building, Energy Build. 70 (2014) 258–270, https://doi.org/10.1016/j.enbuild.2013.11.071.

[12] W. Yang, J. Kuckelkorn, F.-Y. Zhao, H. Spliethoff, Indoor environment of a classroom in a passive school building with displacement ventilation, in: 13th Conference Int. Build. Performances Simul. Assoc., 2013. Chambéry, France.

[13] M.H. Fathollahzadeh, G. Heidarinejad, H. Pasdarshahri, Prediction of thermal comfort, IAQ, and energy consumption in a dense occupancy environment with the under floor air distribution system, Build. Environ. 90 (2015) 96–104, https://doi.org/10.1016/j.buildenv.2015.03.019.

[14] S. Shokrollahi, M. Hadavi, G. Heidarinejad, H. Pasdarshahri, Multi-objective optimization of underfloor air distribution (UFAD) systems performance in a densely occupied environment: a combination of numerical simulation and Taguchi algorithm, J. Build. Eng. 32 (2020), 101495, https://doi.org/10.1016/j.jobe.2020.101495.

[15] M. Mirzaie, E. Lakzian, A. Khan, M.E. Warkiani, O. Mahian, G. Ahmadi, COVID-19 spread in a classroom equipped with partition–A CFD approach, J. Hazard Mater. 420 (2021), 126587, https://doi.org/10.1016/j.jhazmat.2021.126587.

[16] M. Abuhegazy, K. Talaat, O. Anderoglu, S.V. Poroseva, K. Talaat, Numerical investigation of aerosol transport in a classroom with relevance to COVID-19, Phys. Fluids 32 (2020), https://doi.org/10.1063/5.0029118.

[17] J. Ye, Z. Ai, C. Zhang, A new possible route of airborne transmission caused by the use of a physical partition, J. Build. Eng. 44 (2021), 103420, https://doi.org/10.1016/j.jobe.2021.103420.

[18] Z. Lin, L. Tian, T. Yao, Q. Wang, T.T. Chow, Experimental and numerical study of room airflow under stratum ventilation, Build. Environ. 46 (2011) 235–244, https://doi.org/10.1016/j.buildenv.2010.07.018.

[19] C. Qin, W. Zhou, H. Fang, W.Z. Lu, E.W. Lee, Optimization of return vent height for stratified air distribution system with impinging jet supply satisfying threshold of |PMV|<0.5, J. Clean. Prod. 359 (2022), 132033, https://doi.org/10.1016/j.jclepro.2022.132033.

[20] L. Wang, X. Dai, J. Wei, Z. Ai, Y. Fan, L. Tang, et al., Numerical comparison of the efficiency of mixing ventilation and impinging jet ventilation for exhaled particle removal in a model intensive care unit, Build. Environ. 200 (2021), 107955, https://doi.org/10.1016/j.buildenv.2021.107955.

[21] C. Qin, S. Wu, H. Fang, W.Z. Lu, The impacts of evaluation indices and normalization methods on E-TOPSIS optimization of return vent height for an impinging jet ventilation system, Build. Simulat. (2022), https://doi.org/10.1007/s12273-022-0914-z.

[22] X. Ye, Y. Kang, Z. Yan, B. Chen, K. Zhong, Optimization study of return vent height for an impinging jet ventilation system with exhaust/return-split configuration by TOPSIS method, Build. Environ. 177 (2020), 106858, https://doi.org/10.1016/j.buildenv.2020.106858.

[23] T. Kobayashi, K. Sugita, N. Umemiya, T. Kishimoto, M. Sandberg, Numerical investigation and accuracy verification of indoor environment for an impinging jet ventilated room using computational fluid dynamics, Build. Environ. 115 (2017) 251–268, https://doi.org/10.1016/j.buildenv.2017.01.022.

[24] J. Hu, Y. Kang, Y. Lu, J. Yu, K. Zhong, Simplified models for predicting thermal stratification in impinging jet ventilation rooms using multiple regression analysis, Build. Environ. 206 (2021), 108311, https://doi.org/10.1016/j.buildenv.2021.108311.

[25] W. Su, B. Yang, A. Melikov, C. Liang, Y. Lu, F. Wang, et al., Infection probability under different air distribution patterns, Build. Environ. 207 (2022), 108555, https://doi.org/10.1016/j.buildenv.2021.108555.

[26] B. Blocken, Computational Fluid Dynamics for urban physics: importance, scales, possibilities, limitations and ten tips and tricks towards accurate and reliable simulations, Build. Environ. 91 (2015) 219–245, https://doi.org/10.1016/j.buildenv.2015.02.015.

[27] S. Gilani, H. Montazeri, B. Blocken, CFD simulation of stratified indoor environment in displacement ventilation: validation and sensitivity analysis, Build. Environ. 95 (2016) 299–313, https://doi.org/10.1016/j.buildenv.2015.09.010.

[28] Z. Liu, W. Zhuang, X. Hu, Z. Zhao, R. Rong, J. Li, et al., Potential infection risk assessment of improper bioaerosol experiment operation in one BSL-3 laboratory based on the improved Wells-Riley method, Build. Environ. 201 (2021), 107974, https://doi.org/10.1016/j.buildenv.2021.107974.

[29] World Health Organisation (WHO), COVID-19 transmission and protective measures. https://www.who.int/westernpacific/emergencies/covid-19/information/transmission-protective-measures, 2022. (Accessed 16 September 2022).

[30] Y. Goh, B.Y.Q. Tan, C. Bhartendu, J.J.Y. Ong, V.K. Sharma, The face mask: how a real protection becomes a psychological symbol during Covid-19? Brain Behav. Immun. 88 (2020) 1–5, https://doi.org/10.1016/j.bbi.2020.05.060.

[31] Z. Ai, C.M. Mak, N. Gao, J. Niu, Tracer gas is a suitable surrogate of exhaled droplet nuclei for studying airborne transmission in the built environment, Build. Simulat. (2020) 489–496, https://doi.org/10.1007/s12273-020-0614-5.

[32] T. Karimipanah, H.B. Awbi, Theoretical and experimental investigation of impinging jet ventilation and comparison with wall displacement ventilation, Build. Environ. 37 (2002) 1329–1342, https://doi.org/10.1016/S0360-1323(01)00117-2.

[33] A.Q. Ahmed, S. Gao, A.K. Kareem, A numerical study on the effects of exhaust locations on energy consumption and thermal environment in an office room served by displacement ventilation, Energy Convers. Manag. 117 (2016) 74–85, https://doi.org/10.1016/j.enconman.2016.03.004.

[34] Y. Fan, X. Li, Y. Yan, J. Tu, Overall performance evaluation of underfloor air distribution system with different heights of return vents, Energy Build. 147 (2017) 176–187, https://doi.org/10.1016/j.enbuild.2017.04.070.

[35] H.J. Chen, B. Moshfegh, M. Cehlin, Numerical investigation of the flow behavior of an isothermal impinging jet in a room, Build. Environ. 49 (2012) 154–166, https://doi.org/10.1016/j.buildenv.2011.09.027.

[36] T. Chen, Z. Feng, S.-J. Cao, The effect of vent inlet aspect ratio and its location on ventilation efficiency, Indoor Built Environ. 29 (2020) 180–195, https://doi.org/10.1177/1420326X19865930.

[37] H.Y. Deng, Z. Feng, S.-J. Cao, Influence of air change rates on indoor CO2 stratification in terms of Richardson number and vorticity, Build. Environ. 129 (2018) 74–84, https://doi.org/10.1016/j.buildenv.2017.12.009.

[38] J. Ai, A.W.K. Law, S.C.M. Yu, On Boussinesq and non-Boussinesq starting forced plumes, J. Fluid Mech. 558 (2006) 357–386, https://doi.org/10.1017/S0022112006000061.

[39] M.J. Cook, Y. Ji, G.R. Hunt, CFD modelling of natural ventilation: combined wind and buoyancy forces, Int. J. Vent. 1 (2003) 169–179, https://doi.org/10.1080/14733315.2003.11683632.

[40] C. Voelker, H. Alsaad, Simulating the human body's microclimate using automatic coupling of CFD and an advanced thermoregulation model, Indoor Air (2018) 415–425, https://doi.org/10.1111/ina.12451.

[41] N. Ismail, D. Ouahrani, Modelling of cooling radiant cubicle for an office room to test cooling performance, thermal comfort and energy savings in hot climates, Energy 244 (2022), 123185, https://doi.org/10.1016/j.energy.2022.123185.

[42] B. Kong, R.D. Vigil, Simulation of photosynthetically active radiation distribution in algal photobioreactors using a multidimensional spectral radiation model, Bioresour. Technol. 158 (2014) 141–148, https://doi.org/10.1016/j.biortech.2014.01.052.

[43] D. Zhang, Y. Cai, D. Liu, F. Zhao, Y. Li, Dual steady flow solutions of heat and pollutant removal from a slot ventilated welding enclosure containing a bottom heating source, Int. J. Heat Mass Tran. 132 (2019) 11–24, https://doi.org/10.1016/j.ijheatmasstransfer.2018.11.121.

[44] E.N. Fuller, P.D. Schettler, J.C. Giddings, A new method for prediction of binary gas-phase diffusion coefficients, Ind. Eng. Chem. 58 (1966) 18–27, https://doi.org/10.1021/ie50677a007.

[45] C. Qin, X. Wang, G. Zhang, Q. Yi, Y. He, K. Wang, Effects of the slatted floor layout on flow pattern in a manure pit and ammonia emission from pit-A CFD study, Comput. Electron. Agric. 177 (2020), 105677, https://doi.org/10.1016/j.compag.2020.105677.

[46] H. Yamasawa, T. Kobayashi, T. Yamanaka, N. Choi, M. Cehlin, A. Ameen, Effect of supply velocity and heat generation density on cooling and ventilation effectiveness in room with impinging jet ventilation system, Build. Environ. (2021), https://doi.org/10.1016/j.buildenv.2021.108299.

[47] J.N. Baléo, P. Le Cloirec, Validating a prediction method of mean residence time spatial distributions, AIChE J. 46 (2000) 675–683, https://doi.org/10.1002/aic.690460403.

[48] ANSYS Inc, ANSYS Fluent Theory Guide, 2015. Pennsylvania.

[49] P. Nielsen, S. Murakami, S. Kato, C. Topp, J.-H. Yang, Benchmark Tests for a Computer Simulated Person, 1–6, Aalborg Univ, 2003.

[50] GB7793, Ministry of Health of People's Republic of China, Standardization Administration of China,Hygienic Standard for Day Lighting and Artificial Lighting for Middle and Elementary School, In Chinese, 2010. Beijing.

[51] GB50736, China Architecture and Building Press, the People's Republic of China National Standard GB 50736-2012, Design Code for Heating, Ventilation and Air Conditioning of Civil Buildings, In Chinese, Bejing, 2012.

[52] ASHRAE 62.1, ANSI/ASHRAE Standard 62.1-2010, Ventilation for Acceptable Indoor Air Quality, Atlanta, USA, 2010.

[53] O. Han, A. Li, Velocity distribution of wall-attached jets in slotted-inlet ventilated rooms, Build. Environ. (2021), https://doi.org/10.1016/j.buildenv.2021.107708.

[54] C. Qin, W.Z. Lu, Effects of ceiling exhaust location on thermal comfort and age of air in room under impinging jet supply scheme, J. Build. Eng. 35 (2021), 101966, https://doi.org/10.1016/j.jobe.2020.101966.

[55] C. Qin, H. Fang, S. Wu, W.Z. Lu, Establishing multi-criteria optimization of return vent height for underfloor air distribution system, J. Build. Eng. 57 (2022), 104800, https://doi.org/10.1016/j.jobe.2022.104800.

[56] C.K. Saha, G. Zhang, J.Q. Ni, Airflow and concentration characterisation and ammonia mass transfer modelling in wind tunnel studies, Biosyst. Eng. 107 (2010) 328–340, https://doi.org/10.1016/j.biosystemseng.2010.09.007.

[57] P.J. Roache, Quantification of uncertainty in computational fluid dynamics, Annu. Rev. Fluid Mech. 123–60 (1997), https://doi.org/10.1146/annurev.fluid.29.1.123.

[58] Z. Lin, T.T. Chow, C.F. Tsang, K.F. Fong, L.S. Chan, Stratum ventilation - a potential solution to elevated indoor temperatures, Build. Environ. 44 (2009) 2256–2269, https://doi.org/10.1016/j.buildenv.2009.03.007.

[59] Q. Chen, K. Hu, Prediction model for SVOCs transport in the air and interactions with airborne particles, Atmos. Environ. 96 (2014) 61–69, https://doi.org/10.1016/j.atmosenv.2014.07.026.

[60] F. Chen, S.C.M. Yu, A.C.K. Lai, Modeling particle distribution and deposition in indoor environments with a new drift-flux model, Atmos. Environ. 40 (2006) 357–367, https://doi.org/10.1016/j.atmosenv.2005.09.044.

[61] A. Foster, M. Kinzel, Estimating COVID-19 exposure in a classroom setting: a comparison between mathematical and numerical models, Phys. Fluids 33 (2021), https://doi.org/10.1063/5.0040755.

[62] W.Z. Lu, A.Y.T. Leung, S.H. Yan, A.T.P. So, A preliminary parametric study on performance of SARS virus cleaner using CFD simulation, Int. J. Numer. Methods Fluid. 47 (2005) 1137–1146.

[63] Y. Wen, J. Leng, X. Shen, G. Han, L. Sun, F. Yu, Environmental and health effects of ventilation in subway stations: a literature review, Int. J. Environ. Res. 17 (3) (2020) 1084.

[64] C.E. Riley, G. Murphy, R.L. Riley, Airborne spread of measles in a suburban elementary school, Am. J. Epidemiol. 107 (1978) 421–432.

[65] C. Wang, S. Holmberg, S. Sadrizadeh, Numerical study of temperature-controlled airflow in comparison with turbulent mixing and laminar airflow for operating room ventilation, Build. Environ. 144 (2018) 45–56, https://doi.org/10.1016/j.buildenv.2018.08.010.

[66] X. Shao, X. Li, COVID-19 transmission in the first presidential debate in 2020, Phys. Fluids (2020), 115125, https://doi.org/10.1063/5.0032847.

[67] P. Cheng, W. Chen, S. Xiao, F. Xue, Q. Wang, P. Wai, et al., Probable cross-corridor transmission of SARS-CoV-2 due to cross airflows and its control, Build. Environ. 218 (2022), 109137, https://doi.org/10.1016/j.buildenv.2022.109137.

[68] X. Li, D. Lester, G. Rosengarten, C. Aboltins, M. Patel, I. Cole, A spatiotemporally resolved infection risk model for airborne transmission of COVID-19 variants in indoor spaces, Sci. Total Environ. 812 (2022), 152592, https://doi.org/10.1016/j.scitotenv.2021.152592.

[69] C. Habchi, K. Ghali, N. Ghaddar, W. Chakroun, S. Alotaibi, Ceiling personalized ventilation combined with desk fans for reduced direct and indirect cross-contamination and efficient use of office space, Energy Convers. Manag. 111 (2016) 158–173, https://doi.org/10.1016/j.enconman.2015.12.067.

[70] A. Makhoul, K. Ghali, N. Ghaddar, Low-mixing coaxial nozzle for effective personalized ventilation, Indoor Built Environ. 24 (2015) 225–243, https://doi.org/10.1177/1420326X13508967.

[71] W. Liu, T. Zhang, Y. Xue, Z. Zhai, J. Wang, Y. Wei, et al., State-of-the-art methods for inverse design of an enclosed environment, Build. Environ. 91 (2015) 91–100, https://doi.org/10.1016/j.buildenv.2015.02.041.

[72] X. Zhao, Q. Chen, Inverse design of indoor environment using an adjoint RNG k-ε turbulence model, Indoor Air (2019) 320–330, https://doi.org/10.1111/ina.12530.

[73] X. Shan, W. Xu, Y.K. Lee, W.Z. Lu, Evaluation of thermal environment by coupling CFD analysis and wireless-sensor measurements of a full-scale room with cooling system, Sustain. Cities Soc. 45 (2019) 395–405, https://doi.org/10.1016/j.scs.2018.12.011.

[74] Y. Zhang, J. Liu, J. Pei, J. Li, C. Wang, Performance evaluation of different air distribution systems in an aircraft cabin mockup, Aero. Sci. Technol. 70 (2017) 359–366, https://doi.org/10.1016/j.ast.2017.08.009.

[75] Y. Cheng, J. Yang, Z. Du, J. Peng, Investigations on the energy efficiency of stratified air distribution systems with different diffuser layouts, Sustain. Times 8 (2016) 732, https://doi.org/10.3390/su8080732.

[76] Y. Cheng, J. Niu, N. Gao, Stratified air distribution systems in a large lecture theatre: a numerical method to optimize thermal comfort and maximize energy saving, Energy Build. 55 (2012) 515–525, https://doi.org/10.1016/j.enbuild.2012.09.021.

[77] P.O. Fanger, Thermal environment- human requirements, Environmentalist 6 (1986) 275–278.

[78] ISO 7730. Ergonomics of the Thermal Environment, Analytical Determination and Interpretation of Thermal Comfort Using Calculation of the PMV and PPD Indices and Local Thermal Comfort Criteria, 2005.

[79] ASHRAE 55. ANSI/ASHRAE Standard 55–2010, Thermal Environmental Conditions for Human Occupancy, Atlanta, Georgia, USA, 2010.

[80] S. Zhang, Z. Ai, Z. Lin, Novel demand-controlled optimization of constant-air-volume mechanical ventilation for indoor air quality, durability and energy saving, Appl. Energy 293 (2021), 116954, https://doi.org/10.1016/j.apenergy.2021.116954.

[81] P. Anand, C. Sekhar, D. Cheong, M. Santamouris, S. Kondepudi, Occupancy-based zone-level VAV system control implications on thermal comfort, ventilation, indoor air quality and building energy efficiency, Energy Build. 204 (2019), https://doi.org/10.1016/j.enbuild.2019.109473.

[82] K. Zhong, X. Yang, Y. Kang, Effects of ventilation strategies and source locations on indoor particle deposition, Build. Environ. 45 (2010) 655–662, https://doi.org/10.1016/j.buildenv.2009.08.003.

[83] C. Liang, X. Li, X. Shao, B. Li, Numerical analysis of the methods for reducing the energy use of air-conditioning systems in non-uniform indoor environments, Build. Environ. 167 (2020), 106442, https://doi.org/10.1016/j.buildenv.2019.106442.
[84] Z. Wang, H. Wang, Z. Pan, Research on screw chiller which has high outlet temperature and its performance, Int. Conf. Multimed. Technol. ICMT (2011), https://doi.org/10.1109/ICMT.2011.6003328, 2011 2011:4535–8.
[85] S. Sayadi, G. Tsatsaronis, T. Morosuk, M. Baranski, R. Sangi, D. Müller, Exergy-based control strategies for the efficient operation of building energy systems, J. Clean. Prod. 241 (2019), 118277, https://doi.org/10.1016/j.jclepro.2019.118277.
[86] M.K. Singh, S. Mahapatra, S.K. Atreya, Adaptive thermal comfort model for different climatic zones of North-East India, Appl. Energy 88 (2011) 2420–2428, https://doi.org/10.1016/j.apenergy.2011.01.019.
[87] S. Zhang, Z. Lin, Adaptive-rational thermal comfort model: adaptive predicted mean vote with variable adaptive coefficient, Indoor Air (2020) 1–11, https://doi.org/10.1111/ina.12665.
[88] P. Tupper, H. Boury, M. Yerlanov, C. Colijn, Event-specific interventions to minimize COVID-19 transmission, Proc. Natl. Acad. Sci. U. S. A. 117 (2020) 32038–32045, https://doi.org/10.1073/pnas.2019324117.